ACS APPLIED MATERIALS & INTERFACES

Research Article

www.acsami.org

Plasma Jet Printing of Electronic Materials on Flexible and Nonconformal Objects

Ram P. Gandhiraman,* Vivek Jayan, Jin-Woo Han, Bin Chen, Jessica E. Koehne, and M. Meyyappan

NASA Ames Research Center, Moffett Field, California 94035, United States

ABSTRACT: We present a novel approach for the room-temperature fabrication of conductive traces and their subsequent site-selective dielectric encapsulation for use in flexible electronics. We have developed an aerosol-assisted atmospheric pressure plasma-based deposition process for efficiently depositing materials on flexible substrates. Silver nanowire conductive traces and silicon dioxide dielectric coatings for encapsulation were deposited using this approach as a demonstration. The paper substrate with silver nanowires exhibited a very low change in resistance upon 50 cycles of systematic deformation, exhibiting high mechanical flexibility. The applicability of this process to print conductive traces on nonconformal 3D objects was also demonstrated through deposition on a 3D-printed thermoplastic object, indicating the potential to combine plasma printing with 3D printing technology. The role of plasma here includes activation of the material present in the aerosol for deposition, increasing the deposition rate, and plasma polymerization in the case of inorganic coatings. The demonstration here establishes a low-cost, high-throughput, and facile process for printing electronic components on nonconventional platforms.

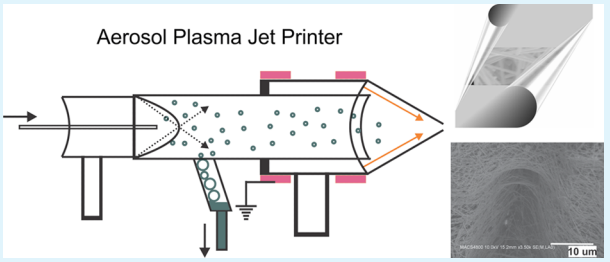

KEYWORDS: *plasma printing, aerosol deposition, PECVD, conductive trace, flexible electronics*

INTRODUCTION

Printing techniques capable of creating a wide range of technologically important components on nonconventional substrates including flexible materials and nonconformal three-dimensional (3D) objects have been of great interest recently but are challenging to develop. Conductive traces and metal electrodes are important parts of all electronic devices. With the rapid growth of interest in flexible electronic devices,[1] paper electronics,[2,3] and wearable devices,[4] there is an urgent need for advanced printing processes that reduce the number of processing steps, material waste, and production cost. The research focus to date has been on inkjet printing,[5,6] solution-based printing,[7,8] dip coating,[9] spin coating,[10] and contact printing.[11,12] Whitesides and colleagues used an aerosol spray deposition[13] process to coat nickel and silver patterns to develop foldable printed circuit boards on paper substrates. The approach, however, produced brittle coatings in addition to flaking when the substrate was bent. Conventional sputtering and evaporation techniques require expensive vacuum-based equipment. They also require masks and/or lithography to perform site-selective deposition, which increases the fabrication cost. In deposition techniques using metal nanocolloids, removing the surfactant at low temperature is a challenging task. Annealing temperatures ranging from 50 to 400 °C have been used for surfactant removal to obtain conductive traces using metal nanostructures.[14−17] Polavarapu et al. printed silver conductive patterns on plastic substrates using the self-aggregating behavior of silver nanoparticles, which behave like a conductive film.[18] All of these techniques typically require multiple processing steps for depositing different materials on the same substrate/device. In addition, a low process temperature is essential when paper or low glass transition temperature plastics are used for substrates.

Park et al.[19] reported very high-resolution printing of a range of nanomaterials using electro hydrodynamic jet printing in which an electric field is used to control fluid flow for printing. While the resolution and versatility of this approach are attractive, the major disadvantage is that the substrate should rest on a metallic support in order to apply a voltage between the nozzle and a conducting support to create electro-hydrodynamic flow of the ink. It is difficult to employ this technique to print on complex 3D objects, and the process is relatively slow.

The need for low-cost, versatile, and high-throughput fabrication processes is growing in electronic device manufacturing. Mechanical flexibility without loss of electronic functionality and performance is a key requirement for flexible electronics devices including foldable displays and wearable devices.[20] We report here stable, well-adherent, and repeatable deposition of electronic materials including conductive nanomaterials and dielectric coatings by aerosol-assisted atmospheric pressure plasma-based printing. As a demonstration, silver nanowire conductive traces are deposited on a range of substrates including cellulose paper, flexible cellulose acetate, and 3D-printed thermoplastic with macroscopically rough features. Sequential deposition of a scratch-resistant dielectric

Received: August 8, 2014
Accepted: November 14, 2014
Published: November 14, 2014

coating on conductive traces is demonstrated as an encapsulation process. This work also shows a pathway for easy integration of nanomaterial printing and atmospheric pressure plasma-enhanced chemical vapor deposition (AP-PECVD) for site-selective deposition and direct patterning without lithography.

EXPERIMENTAL SECTION

Silver Nanowire Deposition. The plasma printing schematic is shown in Figure 1. The atmospheric plasma print head comprises (1) a concentric quartz spray nebulizer (Meinhard concentric quartz nebulizer TQ-50-C1) with a fluid uptake of 1 SLPM; (2) a spray chamber complete with a drain located at the base with inlet diameter of 10 mm, outlet diameter of 9 mm, and a drain diameter of 9 mm; and (3) a spray nozzle equipped with two copper electrodes spaced approximately 2 cm apart. The nozzle diameter is 4 mm, and the length of the spray nozzle is 70 mm. Two pieces of copper tape wound over the spray nozzle serve as concentric outer electrodes. A PVM400 high-voltage (1−15 kV), high-frequency (20−50 kHz) plasma driver (Information Unlimited, Amherst, NH, USA) is used as a power supply.

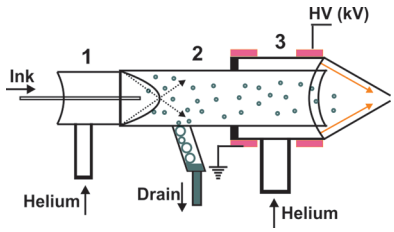

Figure 1. Schematic of the plasma printing system.

Helium is the primary gas source for igniting and sustaining the plasma. Preliminary experiments with argon yielded an unstable plasma, characterized by high-current filaments with streamers. However, helium provides stable plasma for the same electrode configuration and gas flow rates. The helium flow through a gas inlet is maintained as the primary gas flow at 2000 sccm, and this gas input line is used for introducing sufficient gas flow to facilitate ignition as well as to focus the spot size. Silver nanowire ink is supplied into the nebulizer via a syringe pump. Concurrently, helium is also flown into the nebulizer via a gas input line as secondary gas flow at 500 sccm. As the ink reaches the tip of the capillary line, it is bombarded by the rapid gas flow, and a fine aerosol mist is formed in the spray chamber. As the mist condenses on the sidewalls of the spray chamber, larger droplets fall into the drain. The finer aerosol particles gain enough momentum to reach the electrode junction. They are shielded from ignition by the inner pyrex tube of the print head. The additional gas is ignited and accelerated through the nozzle of the print head. The heavier droplets accumulate over the drain of the spray chamber until the negative pressure at the end of the capillary line of the drain pulls out the excess ink. This ink can be recovered by collecting it in a beaker or another container. The aerosolized ink is introduced to the high-energy plasma jet and accelerated out of the nozzle to a relatively fine spot size. The spot size can be adjusted by altering the print head nozzle's diameter.

Dielectric Deposition. Tetraethyl orthosilicate (TEOS) precursor from Sigma-Aldrich was used for the dielectric silicon dioxide coating. TEOS was placed in a round-bottomed flask, and an ultrasonic nebulizer was used to create the TEOS aerosol, which was then carried into the print head through a secondary helium gas flow. While maintaining the primary gas flow at 2000 sccm, the secondary flow into the nebulization system was kept low, at 50 sccm, to enable transportation of aerosol into the print head and to stop the liquid droplets from reaching the plasma.

Silver Nanowire Synthesis. The silver nanowire synthesis was carried out using the polyol process described by Netzer et al.[21] and Sun et al.[22] Silver nitrate ($AgNO_3$), ethylene glycol (EG) (Fischer Scientific), and poly(vinylpyrrolidone) (PVP) (Alfa Aesar) were the raw materials. A PVP solution was prepared by dissolving 0.6 g of PVP in 30 mL of EG followed by heating to 160 °C for 1 h. An $AgNO_3$ solution in EG was prepared by adding 0.31 g of $AgNO_3$ into 15 mL of EG with constant stirring followed by addition of this to the PVP solution, resulting in the formation of silver nanowires. The NWs were then centrifuged and washed several times to remove PVP and were suspended in methanol.

Characterization. Scanning electron microscopy (SEM) imaging was performed using S4800 scanning electron microscope (Hitachi, Pleasanton, CA). Imaging of the plasma-treated substrates was carried out without any external conductive coating. Untreated cellulose paper was imaged with a conductive carbon coating applied to prevent charging of the substrate while imaging. The nature of chemical bonding in the silicon dioxide dielectric coating was determined using a PerkinElmer Spectrum GX FTIR. An average of 100 scans were used for each spectrum. As the substrate needs to be infrared-transparent, the dielectric coatings were deposited on a silicon wafer. An uncoated silicon wafer was used as the background for measurement. The current−voltage (I−V) characteristics were measured using a semiconductor parameter analyzer (Agilent 4156B). A two-terminal

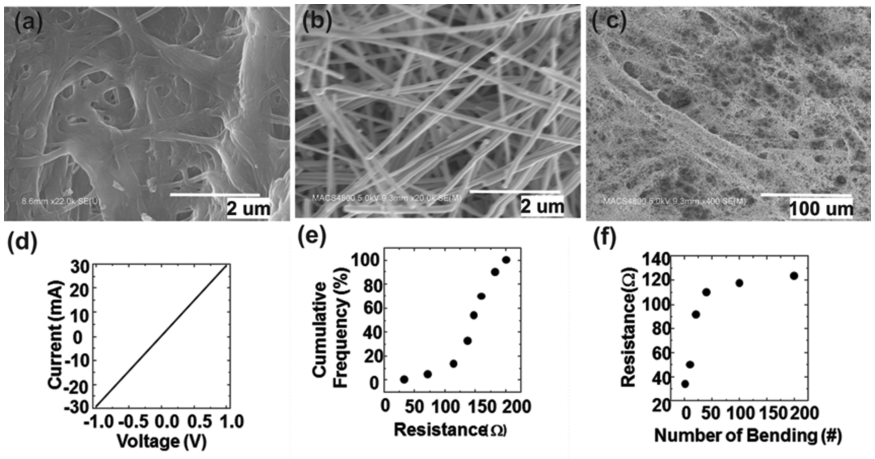

Figure 2. SEM images of (a) untreated cellulose paper substrate (scale 2 μm), (b) plasma-printed silver nanowire conductive traces on cellulose paper (scale, 2 μm), (c) plasma-printed silver nanowire conductive traces on cellulose paper (scale, 100 μm), (d) current−voltage characteristics of silver nanowires deposited on cellulose substrate, (e) resistance vs cumulative frequency plot of silver nanowires on paper, and (f) variation of resistance upon repeated bending.

tungsten tip was used for the contact, and the electrode distance was fixed at 1 mm. In order to investigate the spatial uniformity, the resistance of samples (about 1 × 1 cm^2) were scanned at 100 different spots.

RESULTS AND DISCUSSION

Figure 1 shows the schematic of the plasma printer. An aerosol carrying at least one of the desired substances for deposition is introduced into a cold plasma jet operated at atmospheric pressure. The deposition takes place as a result of the interaction of the aerosol containing the precursor material, with the plasma jet ignited using helium as the primary gas. The role of plasma in the printing process, as will be shown later, includes activation of the material, present in the aerosol, to be deposited and the surface to be coated, increasing the deposition rate, and plasma polymerization in the case of inorganic coatings.

Figure 2a shows an SEM image of unmodified cellulose paper containing microfibers. Figure 2b,c shows the SEM images of silver nanowires deposited on paper using plasma printing. In Figure 2c (at lower magnification, 100 μm), the uniform coverage of cellulose fibers with silver nanowires is clearly seen. The $I-V$ curve in Figure 2d shows ohmic characteristics, confirming the metallic properties of the printed film. Figure 2e shows the spatial distribution of the resistance on the same sample. In order to investigate the spatial uniformity, the resistance of samples of about 1 × 1 cm^2 were scanned over 100 different spots. The mean resistance was approximately 130 Ω, with a standard deviation of 55 Ω. This deviation is due to manual deposition with no automatic control, and the uniformity can be further improved by a controlled deposition method.

It is important to establish the need for the plasma by a direct comparison; therefore, a set of control samples was processed with no plasma but with the same gas flow ratios and deposition time. The mean resistance of the non-plasma-deposited sample was 2.4 kΩ, with a standard deviation of 1.1 kΩ, which is 1 order of magnitude less conductive and uniform than that of the plasma-printed samples. The plasma-assisted printing results in higher conductivity with better uniformity over that of non-plasma printing for the same process conditions. A high-temperature sintering process is usually necessary in aerosol jet printing to densify the material and to remove the surfactant. Such processing steps not only increase the cost and throughput but also limit the use of potential substrates. For example, ordinary paper cannot endure the severity of the sintering process. In contrast, the surfactant is spontaneously removed right before sitting on the substrate in the plasma method, without requiring any postprocessing. Therefore, plasma-assisted printing can be advantageously contrasted with that of aerosol jet printing. It is possible to obtain a highly conductive surface made of silver nanowires through techniques such as drop casting and plain aerosol methods, but this occurs only with a prolonged deposition time, use of a higher quantity of colloids, and post-thermal treatment. However, plasma-assisted deposition enables high-throughput printing with reduced processing time and cost.

The ability of the printed substrates to withstand bending without degradation and loss of electrical characteristics, i.e., electrical robustness, is very important for flexible electronics. The resistance to degradation with repeated bending needs to be established, and Figure 2f shows the resistance change upon cumulative bending cycles. The electrical continuity of the present 2D films is established from the network of individual silver nanowires. When such a networked film suffers from extrinsic mechanical stress, the network structure can be broken. The silver nanowires are in contact with neighboring nanowires by van der Waals forces. Once the extrinsic mechanical force from bending overwhelms the adhesion force, the nanowires can be separated, which can increase the total resistance. In the worst case, the film can be electrically open. However, the present film retains its conductive properties due to the nature of the network. Although a local loss in the connection can be found, the electrical pathway can be maintained through the neighbor nanowires. The resistance increased as the bending was repeated up to 50 times, but it saturated afterward, which suggests that the overall silver nanowire networks become stable and are no longer affected by the external stress. This can be thought of as a conditioning process through some number of initial cycles. The total degradation caused by the stress in the early cycles is 400%, but the resistance value may still be reasonable for use with interconnects and other similar needs. When the printed area was increased from 1 × 1 cm^2 to 1 × 2.5 cm^2, we observed that the resistance measured between two different points separated by 2.5 cm was close to 800 Ω. We speculate that the higher resistance observed for a larger area is probably due to lower loading of nanowires caused by the manual movement of the print head. Controlled and uniform deposition could be achieved with automated movement of the plasma jet or substrate.

Silicon dioxide, the most widely used material for the interlayer dielectric and gate oxide in integrated circuit manufacturing, was also deposited on a flexible cellulose acetate transparent substrate coated with silver nanowires to demonstrate electrical encapsulation and passivation at room temperature. Unlike the printing of nanostructures wherein plasma is used to activate the nanostructures and enhance the deposition, the plasma deposition of a dielectric coating here involves PECVD at atmospheric pressure, resulting in plasma polymerization. In the plasma OFF stage, the organo silane precursor flow will not result in a polymerized film because an external source of energy (heat, laser, or plasma) is required to form a cross-linked network. Plasma acts here as a room-temperature activation source for creating highly reactive radicals, ions, and neutral species that would enable plasma polymerization.

A transparent cellulose acetate sheet was patterned with silver nanowires to form conductive traces with dimensions of 2.5 × 1 cm^2. Silicon dioxide dielectric was deposited in the middle of the silver nanowire pattern, leaving both ends of the conductive trace exposed. The schematic for this encapsulation is shown in Figure 3. Flexible electronics require the electronic components to function without loss of properties after stretching, folding, and heavy deformation. The cellulose fibers deposited with silver nanowires were deformed to various shapes, as shown in Figures 3b–d, and the electrical connectivity was tested under every deformation condition and found to stay intact upon heavy deformation, demonstrating the robustness of the process.

The resistance measured at various locations across the 2.5 cm long conductive trace in the cellulose acetate sheet exhibited variations from 1580 to 1800 Ω. Unlike the paper substrates, the resistance of the transparent cellulose acetate sheet is higher by a factor of 2. We speculate that the loading efficiency is different on different substrates depending on the roughness of

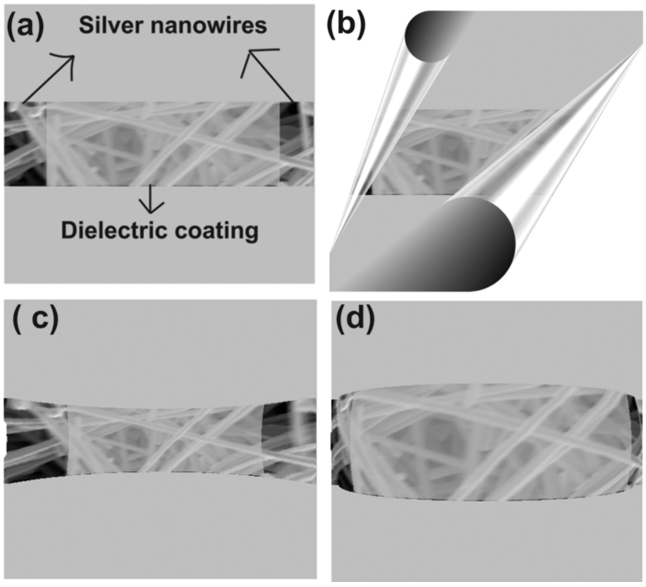

Figure 3. (a) Schematic showing silver nanowire printing on a flexible substrate and encapsution of the printed pattern using a dielectric coating. (b–d) Schematic showing the deformation of the printed plasma and encapsulated features.

the texture. The cellulose fibers on paper enable a higher loading of nanowires due to the porous nature of the surface, as shown in Figure 2a, and the relatively smooth transparent cellulose acetate sheet results in a lower loading of nanowires. We also speculate that differences in treatment time and manual error could contribute to the loading efficiency, both of which can be precisely controlled once the process is automated.

In order to study the influence of plasma on the deposition, we deposited silver nanowires on the cellulose acetate sheets without turning on the plasma while retaining all other experimental conditions the same. The deposition under plasma OFF conditions mimics spray deposition, resulting in poor-quality films compared to those prepared with plasma ON. The resistance measured between the ends of the conductive trace in spray deposition is 3 orders of magnitude higher (1.67 MΩ with plasma-OFF) than that of the plasma-deposited samples. Very high resistance is a result of a lower deposition rate. The role of plasma here includes activation of the material in the aerosol to coat the surface and increase the deposition rate. In non-plasma aerosol deposition, the particles maintain their velocity, acquired by momentum transfer from the carrier gas. However, when the plasma is ON, the particles in the aerosol pick up additional momentum from the highly accelerated plasma gas.[23] The helium plasma at atmospheric pressure has a high electron density (10^{11} cm^{-3}), and the atmospheric pressure discharge is efficient in charging the aerosols, which in turn depends on the electric field, ion density, and transit time.[24−26] Because the silver nanowires are suspended in organic solvent, transient charging is possible, resulting in drifting of the ions on the field lines and enabling increased deposition due to the presence of an electric field. Space charge repulsions also need to be taken into account.

FTIR spectroscopy was employed to analyze the chemical structure of the silicon dioxide dielectric layer. The FTIR spectra of the coating in Figure 4 for various deposition times show that the resultant film is $SiO_xC_yH_z$ in nature. The spectra can be divided into two regions: between 800 to 1200 cm^{-1} and

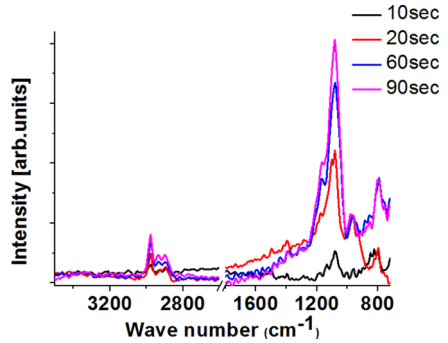

Figure 4. FTIR spectroscopic measurement of silicon dioxide dielectric layers coated over different durations of time. The peak intensities increase with time.

2800 to 3000 cm^{-1}. The multiple bands between 2800 and 3000 cm^{-1} arise from the C−H vibrations in the ethyl components of the TEOS precursor, and the intense bands between 800 and 1200 cm^{-1} arise from Si−O molecular vibrations of the ortho silicate component of the precursor. Details of the peak attribution are given below.

The peaks at 2982 and 2900 cm^{-1} correspond to the asymmetric and symmetric stretching vibrations of C−H in CH_3, respectively. In the same region, the peaks at 2936 cm^{-1} and a shoulder at 2878 cm^{-1} are attributed to the asymmetric and symmetric stretching vibrations of C−H in CH_2, respectively.[27] This is in agreement with the observations of Aumaille et al. on plasma-polymerized SiOCH films using TEOS precursor by low-pressure PECVD.[28] The Si−O bonds are present as both Si−O−C and Si−O−Si. The highly intense peak at 1080 cm^{-1} with a shoulder around 1103 cm^{-1} corresponds to the asymmetric stretching vibration of Si−O−Si and Si−O−C.[29] A sharp peak at 795 cm^{-1} corresponds to the Si−O−Si bending vibration, and the small intensity peaks between 800 and 850 cm^{-1} correspond to hydrocarbon content. The peaks at 1165 and a shoulder around 1203 cm^{-1} to the Si−O bond are attributed to the disorder-induced mechanical coupling of two asymmetric stretching vibrations.[30] The presence of these peaks agrees with the observations by Förch et al. on FTIR analysis of plasma-polymerized films.[31] The peak intensities show a clear rise with deposition time, which has a linear relation to film thickness. It is evident that the asymmetric stretching mode exhibits a pronounced thickness dependence of the full width at half-maximum. The increase in the Si−O−Si asymmetric stretching vibration intensity with deposition time and in turn the film thickness reflect the increased number of different vibration energies in the thicker film.[32] As the film density and refractive index are known to decrease due to the presence of hydrocarbons, the surface composition and hence the optical characteristics can be tailored by incorporating oxygen in the plasma.[33,34] As the exact peak position depends on the film stress, porosity, and composition, changes can be observed in the FTIR spectra. The plasma polymerization results in formation of an amorphous $SiO_xC_yH_z$ film, the composition of which could be tailored by controlling the plasma process parameters such as precursor gas flow rate, power, deposition time, applied potential, nature of the plasma source (pulsed DC, DC, RF), external bias voltage to the substrate, electrode geometry, and substrate temperature. Detailed investigation of the influence of all of these parameters on film characteristics is beyond the scope of current work and can be investigated in future work.

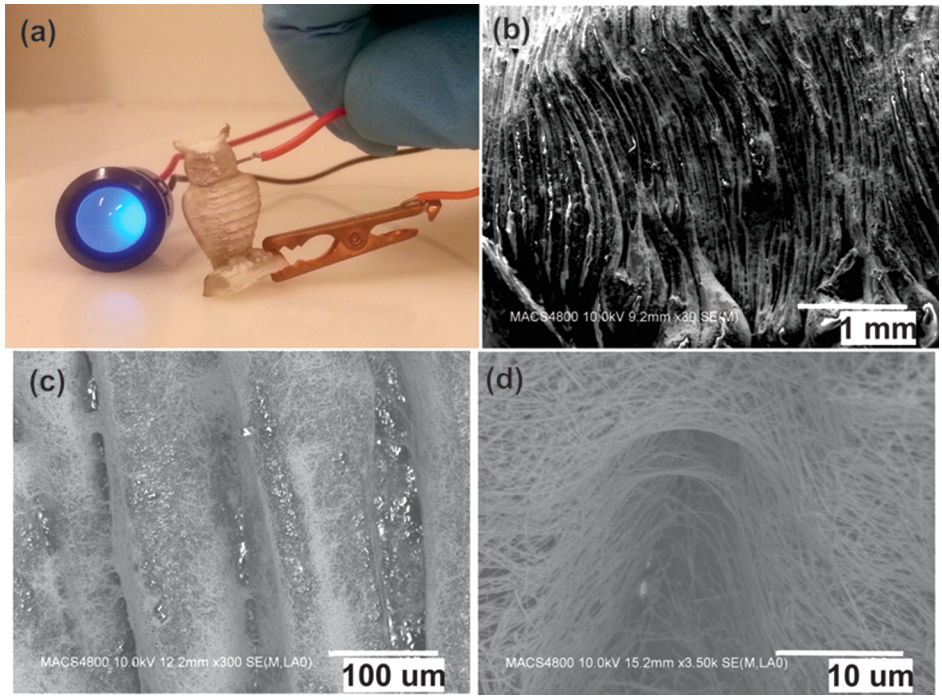

Figure 5. Deposition of silver nanowire conductive patterns on a 3D printed owl made of thermo plastic material. (a) A conductive trace made of silver nanowire is printed along the sides of the owl, and an LED connected to a 9 V battery is lit using the silver nanowires as a conductive path. (b–d) SEM images of a section of a 3D-printed owl containing plasma-printed silver nanowires at three different magnifications.

Recently, 3D printing has been recognized as having tremendous potential to revolutionize future manufacturing processes. We demonstrate here plasma printing of conductive traces on a rough nonuniform 3D-printed object made of acrylonitrile butadiene styrene (ABS) thermoplastic. Figure 5 shows the silver nanowire conductive traces deposited on a 3D-printed thermoplastic. Low-temperature deposition of conductive traces and/or nanostructured materials on complex 3D features with macroscopic rough topographical features is a challenging task. Deposition of conductive traces at room temperature on 3D-printed nonconformal objects can enable unprecedented applications for the rapidly growing technology of 3D printing. A 3D-printed owl made of ABS plastic shown in Figure 5a is patterned with silver nanowires to create conductive paths on the insulating plastic. An LED is lit using a 9 V battery through this silver nanowire conductive path in Figure 5a. The SEM images in Figures 5b–d show macroscopic rough features and a nonconformal shape of the thermoplastic. Also, the SEM images reveal silver nanowires deposited on top of the rough features of the 3D printed owl.

An important feature of plasma printing that is unattainable by other existing printing technologies can be understood by carefully observing the SEM images in Figure 5c,d. The plasma-printed silver nanowires form a highly interlinked network covering both shallow and deep gaps between the plastic fibers. The silver nanowires also get deposited on completely nonplanar complex shapes without losing electrical connectivity. The LED connected between the traces shows that the connectivity between different regions is very good. The adhesion of the silver nanowires on these rough or uneven surfaces is very good.

The conductive pattern on the 3D-printed owl's surface maintained its electrical connectivity and conductivity for more than 8 months of storage in air. The measured electrical resistance, after storage in air for 8 months, showed a very low resistance of 50 Ω over 1 cm separation, confirming that the plasma-printed silver nanowires have good stability. As thin silver films are prone to oxidation and corrosion, we have previously demonstrated low-pressure plasma-based protective and functional coating for retaining their plasmonic properties without aging.[35] The long-term stability of the silver nanowires here, beyond the current 8 months, needs further investigation, as stable material can be exploited for several applications including plasmonic-enhanced organic photovoltaics and surface plasmon resonance-based biosensing in addition to flexible electronics, printing of interconnects, metal plating, and others.

The above results demonstrate that conductive traces or any other nanostructured material with tailored properties could be deposited over complex features, steps, and other irregularities and retain good continuity. Once automated, this technology could be used as a single tool to print and pattern several combinations of materials that are essential for electronic device fabrication. It is possible to have multiple jets, as we have already developed this (details not given here). The ease with which plasma printing could be built and its use in the 3D printing process show that this process could be integrated with 3D printing in which one could stop the polymer definition at certain points, put in a patterned conductive layer, resume deposition, add more wires, and so on.

The silver nanostructures, when embedded at the donor–acceptor interface of the organic heterojunction in solar cell devices, can enhance photon absorption, charge separation, and eventually charge collection through localized surface plasmon resonance (LSPR).[36,37] As the LSPR requires noble metal nanostructures, conventional vacuum-based coating processes require an additional patterning step. Currently, electrodeposition is used to deposit silver nanostructures for heterojunctions in organic solar cell devices.[38] As plasma printing is a solventless process capable of site-selective deposition, the technology presented in this work could be

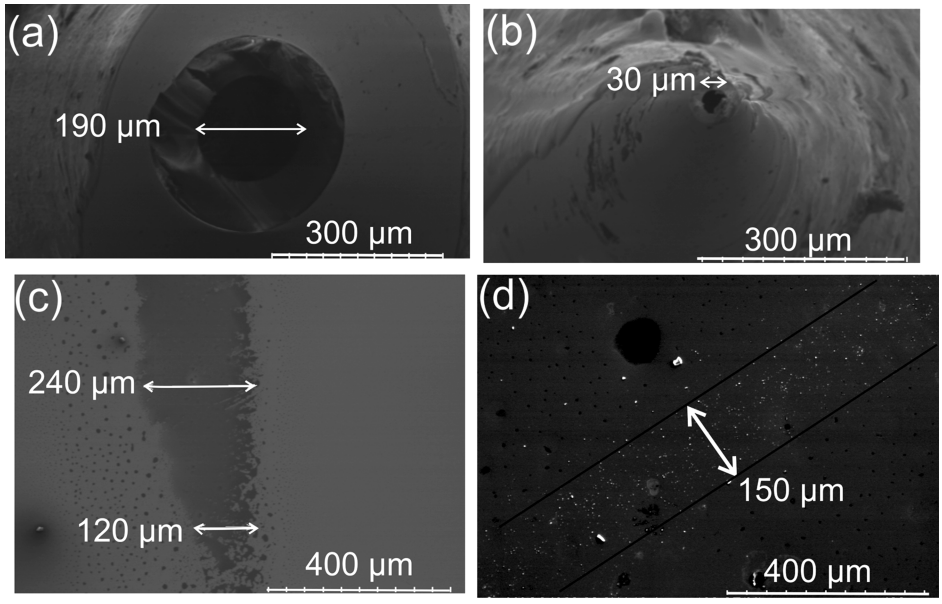

Figure 6. SEM images of (a) a 190 μm diameter micronozzle, (b) a 30 μm diameter micronozzle, (c) a plasma-deposited PVP coating, and (d) plasma-printed silver nanoparticles.

used to print plasmonic nanostructures at the heterojunction and improve the performance of organic photovoltaics. Garnett et al. demonstrated that small gaps formed between silver nanowire junctions enable effective light concentration and produce localized heating, resulting in self-limiting plasmonic welding.[39] It is possible to tailor the density of packing with plasma printing, resulting in the controlled loading of metal nanostructures.

In order to understand the resolution capability of plasma printing, deposition was done using nozzles of different diameters and microjet plasmas. We used two different nozzle diameters, 150 and 30 μm, as shown in the SEM images in Figure 6a,b, respectively. We deposited poly(vinylpyrrolidone) (PVP) (a solvent used in the silver nanowire synthesis) and silver nanoparticles as shown in Figure 6c,d in order to study the resolution capability of the plasma jet for printing both nanomaterials and organic/inorganic coatings. PVP was chosen for its ease of observation under SEM, as a silicon dioxide coating cannot be easily differentiated; highly viscous PVP rapidly forms a thicker coating compared to that with silicon dioxide. Figure 6c shows plasma printing of the PVP that is patterned 120−240 μm wide. The reason for using silver nanoparticles instead of silver nanowires is to study the density of packing and uniformity of the coating process as explained below. The silver nanoparticles were patterned for a width less than 150 μm, as shown in Figure 6d. As the substrate movement was done here manually, we believe that higher resolution is possible with precise control of substrate movement through automated $X-Y$ stage and the distance between the electrode and substrate. The resolution can be controlled by changing the plasma process parameters including gas flow ratios, voltage level, distance between the plasma jet and substrate holder, configuration of electrode, nozzle diameter, and others. Cho et al. and Kim et al. reported a line width resolution as low as 10 μm for aerosol jet printing (without plasma) of electronically functional inks.[40,41]

The deposition uniformity depends on the area and the nanomaterial concentration in the solution. As our focus here is on small-area coating, deposition uniformity for areas exceeding 2.5 cm^2 was not carried out. However, the uniformity over small areas depends on the size and nature of the nanostructured material. For example, a highly uniform coating results, as shown in Figure 2c, with highly concentrated silver nanowires; in contrast, the uniformity is not satisfactory with low concentrations. The SEM image in Figure 6d shows silver nanoparticles deposited within a 100 μm confinement, where the density of packing is much lower compared to that of the silver nanowire deposition in Figure 2c. The density of packing depends on several factors including deposition time, plasma process parameters, distance between the electrode and the substrate, and, more importantly, the concentration of the solution. It is evident from Figures 2c and 6d that the concentration of the nanomaterial in the colloid is very crucial to obtain a uniform coating with a high density of packing. The aerosol formation from the colloid is also critical for uniform deposition, as the presence of large droplets will lead to a large splat.

As the technology develops, two important issues, namely, the blocking of the nozzle and contamination, need to be considered. The blocking effect depends on the type of nanomaterial and also on the nature of the solvent and thus, can be prevented or minimized by judicious choices. Three different organic solvents including PVP, ethanol, and ethylene glycol were used here for suspending the silver nanowires. PVP, being highly viscous, resulted in blocking during deposition. However, no blocking was observed for the low-viscosity ethanol and ethylene glycol suspensions. Deposition of oxidized MWCNTs suspended in water (not reported in this study) resulted in severe blockage of the capillary. The blocking of the capillary depends on the nature, size, and structure of the nanomaterial; for example, silver nanoparticles and nanowires have no/low blocking, and carbon nanotubes exhibit severe blocking. Also, it depends on the viscosity and nature of the suspension used. The best possible way to minimize contamination is to use different nozzle jets for different materials. Sequential deposition using multiple jets has proven to be more effective than that using a single plasma jet.

CONCLUSIONS

We have developed an aerosol-assisted atmospheric pressure plasma-based process as a rapid and cost-effective printing technology. Site-selective deposition of materials, the ability to perform encapsulation, integration of the process, and good mechanical flexibility of the printed substrates without loss of functionality are attractive features of this highly versatile technique. The deposition of a conductive pattern on a macroscopically rough, nonconformal, 3D-printed thermoplastic material shown here is a key success. The silver nanowire-deposited cellulose substrate shows a very low resistance change upon bending 50 times, exhibiting very high mechanical flexibility, and the resistance saturated after 50 cycles. The role of plasma in the printing process includes activation of the material, increasing the deposition rate, and plasma polymerization in the case of inorganic coatings. The ability to deposit a wide range of materials, e.g., metal or oxides, conducting, semiconducting, or insulating, with precise control over the material characteristics offers several advantages over conventional printing technology.

AUTHOR INFORMATION

Corresponding Author

*E-mail: ramprasad.gandhiraman@nasa.gov. Telephone: (650) 604-4702.

Notes

The authors declare no competing financial interest.

ACKNOWLEDGMENTS

R.P. Gandhiraman is with Universities Space Research Association, subcontracted to NASA Ames Research Center under a NASA cooperative agreement.

REFERENCES

(1) Secor, E. B.; Prabhumirashi, P. L.; Puntambekar, K.; Geier, M. L.; Hersam, M. C. Inkjet Printing of High Conductivity, Flexible Graphene Patterns. *J. Phys. Chem. Lett.* **2013**, *4*, 1347−1351.

(2) Han, J. W.; Kim, B.; Li, J.; Meyyappan, M. A Carbon Nanotube Based Ammonia Sensor on Cellulose Paper. *RSC Adv.* **2014**, 549−553.

(3) Huang, J.; Zhu, H.; Chen, Y.; Preston, C.; Rohrbach, K.; Cumings, J.; Hu, L. Highly Transparent and Flexible Nanopaper Transistors. *ACS Nano* **2013**, *7*, 2106−2113.

(4) Han, J. W.; Kim, B.; Li, J.; Meyyappan, M. A Carbon Nanotube Based Ammonia Sensor on Cotton Textile. *Appl. Phys. Lett.* **2013**, *102*, 193104.

(5) Sirringhaus, H.; Kawase, T.; Friend, R. H.; Shimoda, T.; Inbasekaran, M.; Wu, W.; Woo, E. P. High-Resolution Inkjet Printing of All-Polymer Transistor Circuits. *Science* **2000**, *290*, 2123−2126.

(6) Wang, S.; Ang, P. K.; Wang, Z.; Tang, A. L.L.; Thong, J. T. L.; Loh, K. P. High Mobility, Printable, and Solution-Processed Graphene Electronics. *Nano Lett.* **2009**, *10*, 92−98.

(7) Hu, L.; Choi, J. W.; Yang, Y.; Jeong, S.; Mantia, F. L.; Cui, L.-F.; Cui, Y. Highly Conductive Paper for Energy-Storage Devices. *Proc. Natl. Acad. Sci. U.S.A.* **2009**, *106*, 21490−21494.

(8) Lee, H. M.; Lee, H. B.; Jung, D. S.; Yun, J.-Y.; Ko, S. H.; Park, S. B. Solution Processed Aluminum Paper for Flexible Electronics. *Langmuir* **2012**, *28*, 13127−13135.

(9) Shim, B. S.; Chen, W.; Doty, C.; Xu, C.; Kotov, N. A. Smart Electronic Yarns and Wearable Fabrics for Human Biomonitoring made by Carbon Nanotube Coating with Polyelectrolytes. *Nano Lett.* **2008**, *8*, 4151−4157.

(10) Kholmanov, I. N.; Magnuson, C. W.; Aliev, A. E.; Li, H.; Zhang, B.; Suk, J. W.; Zhang, L. L.; Peng, E.; Mousavi, S. H.; Khanikaev, A. B.; Piner, R.; Shvets; Ruoff, R. S. Improved Electrical Conductivity of Graphene Films Integrated with Metal Nanowires. *Nano Lett.* **2012**, *12*, 5679−5683.

(11) Fan, Z. Y.; Ho, J. C.; Jacobson, Z. A.; Yerushalmi, R.; Alley, R. L.; Razavi, H.; Javey, A. Wafer-Scale Assembly of Highly Ordered Semiconductor Nanowire Arrays by Contact Printing. *Nano Lett.* **2008**, *8*, 20−25.

(12) Takahashi, T.; Takei, K.; Ho, J. C.; Chueh, Y. L.; Fan, Z.; Javey, A. Monolayer Resist for Patterned Contact Printing of Aligned Nanowire Arrays. *J. Am. Chem. Soc.* **2009**, *131*, 2102−2103.

(13) Siegel, A. C.; Philips, S. T.; Dickey, M. D.; Lu, N.; Suo, Z.; Whitesides, G. M. Foldable Printed Circuit Boards on Paper Substrates. *Adv. Funct. Mater.* **2010**, *20*, 28−35.

(14) Anto, B. T.; Sivaramakrishnan, S.; Chua, L. L.; Ho, P. K. H. Hydrophilic Sparse Ionic Monolayer-Protected Metal Nanoparticles: Highly Concentrated Nano-Au and Nano-Ag "Inks" That Can Be Sintered to Near-Bulk Conductivity at 150 °C. *Adv. Funct. Mater.* **2010**, *20*, 296−303.

(15) Van Osch, T. H. J.; Perelaer, J.; de Laat, A. W. M.; Schubert, U. S. Inkjet Printing of Narrow Conductive Tracks on Untreated Polymeric Substrates. *Adv. Mater.* **2008**, *20*, 343−345.

(16) Magdassi, S.; Grouchko, M.; Berezin, O.; Kamyshny, A. Triggering the Sintering of Silver Nanoparticles at Room Temperature. *ACS Nano* **2010**, *4*, 1943−1948.

(17) Kim, D.; Jeong, S.; Shin, H.; Xia, Y.; Moon, J. Heterogeneous Interfacial Properties of Ink-Jet-Printed Silver Nanoparticulate Electrode and Organic Semiconductor. *Adv. Mater.* **2008**, *20*, 3084−3089.

(18) Polavarapu, L.; Manga, K. K.; Cao, H. D.; Loh, K. P.; Xu, Q.-H. Preparation of Conductive Silver Films at Mild Temperatures for Printable Organic Electronics. *Chem. Mater.* **2011**, *23*, 3273−3276.

(19) Park, J. U.; Hardy, M.; Kang, S. J.; Barton, K.; Adair, K.; Mukhopadhyay, D. K.; Lee, C. Y.; Strano, M. S.; Alleyne, A. G.; Georgiadis, J. G.; Ferreira, P. M.; Rogers, J. A. High-Resolution Electrohydrodynamic Jet Printing. *Nat. Mater.* **2007**, *6*, 782−789.

(20) Sekitani, T.; Zschieschang, U.; Klauk, H.; Someya, T. Flexible Organic Transistors and Circuits with Extreme Bending Stability. *Nat. Mater.* **2010**, *9*, 1015−1022.

(21) Netzer, N. L.; Qiu, C.; Zhang, Y.; Lin, C.; Zhang, L.; Fong, H.; Jiang, C. Gold−Silver Bimetallic Porous Nanowires for Surface-Enhanced Raman Scattering. *Chem. Commun.* **2011**, *47*, 9606−9608.

(22) Sun, Y. G.; Gates, B.; Mayers, B.; Xia, Y. N. Crystalline Silver Nanowires by Soft Solution Processing. *Nano Lett.* **2002**, *2*, 165−168.

(23) Heimann, R. B. *Plasma Spray Coating: Principles and Applications*, 2nd ed; Wiley-VCH: Weinheim, Germany, 2008.

(24) Moravej, M.; Yang, X.; Nowling, G. R.; Chang, J. P.; Hicks, R. F.; Babayan, S. E. Physics of High-Pressure Helium and Argon Radio-Frequency Plasmas. *J. Appl. Phys.* **2004**, *96*, 7011−7017.

(25) Borra, J. P. Charging of Aerosol and Nucleation in Atmospheric Pressure Electrical Discharges. *Plasma Phys. Controlled Fusion* **2008**, *50*, 124036.

(26) Jidenko, N.; Jimenez, C.; Massines, F.; Borra, J.-P. Nano-Particle Size-Dependent Charging and Electro-Deposition in Dielectric Barrier Discharges at Atmospheric Pressure for Thin SiO_x Film Deposition. *J. Phys. D: Appl. Phys.* **2007**, *40*, 4155−4163.

(27) Kurth, D. G.; Thomas, B. Thin Films of (3-Aminopropyl)-triethoxysilane on Aluminum Oxide and Gold Substrates. *Langmuir* **1906**, *11*, 3061−3067.

(28) Aumaille, K.; Vallee, C.; Granier, A.; Goullet, A.; Gaboriau, F.; Turban, G. A Comparative Study of Oxygen/Organosilicon Plasmas and Thin $SiO_xC_yH_z$ Films Deposited in a Helicon Reactor. *Thin Solid Films* **2000**, *359*, 188−196.

(29) Socrates, G. *Infrared and Raman Characteristic Group Frequencies*, 3rd ed; John Wiley and Sons Ltd.: Chichester, UK, 2004.

(30) Kirk, C. T. Quantitative Analysis of the Effect of Disorder-Induced Mode Coupling on Infrared Absorption in Silica. *Phys. Rev. B* **1988**, *38*, 1255−1273.

(31) Förch, R.; Chifen, A. N.; Bousquet, A.; Khor, H. L.; Jungblut, M.; Chu, L.-Q.; Zhang, Z.; Osey-Mensah, I.; Sinner, E.-K.; Knoll, W.

Recent and Expected Roles of Plasma-Polymerized Films for Biomedical Applications. *Chem. Vap. Deposition* **2007**, *13*, 280−294.
(32) Bensch, W.; Bergholz, W. An FT-IR Study of Silicon Dioxides for VLSI Microelectronics. *Semicond. Sci. Technol.* **1990**, *5*, 421−428.
(33) Kim, H. J.; Shao, Q.; Kim, Y.-H. Characterization of Low-Dielectric-Constant SiOC Thin Films Deposited by PECVD for Interlayer Dielectrics of Multilevel Interconnection. *Surf. Coat. Technol.* **2003**, *171*, 39−45.
(34) Babayan, S. E.; Jeong, J. Y.; Schutze, A.; Tu, V. J.; Moravej, M.; Selwyn, G. S.; Hick, R. F. Deposition of Silicon Dioxide Films with a Non-equilibrium Atmospheric Pressure Plasma Jet. *Plasma Sources Sci. Technol.* **2001**, *10*, 573−578.
(35) Manickam, G.; Gandhiraman, R. P.; Vijayaraghavan, R. K.; Kerr, L.; Doyle, C.; Williams, D. E.; Daniels, S. Protection and Functionalisation of Silver as an Optical Sensing Platform for Highly Sensitive SPR Based Analysis. *Analyst* **2012**, *137*, 5265−5271.
(36) Thomann, I.; Pinaud, B. A.; Chen, Z.; Clemens, B. M.; Jaramillo, T. F.; Brongersma, M. L. Plasmon Enhanced Solar-to-Fuel Energy Conversion. *Nano Lett.* **2011**, *11*, 3440−3446.
(37) Schuller, J. A.; Barnard, E. S.; Cai, W.; Jun, Y. C.; White, J. S.; Brongersma, M. L. Plasmonics for Extreme Light Concentration and Manipulation. *Nat. Mater.* **2010**, *9*, 193−204.
(38) Kim, S.-S.; Na, S.-I.; Jo, J.; Kim, D.-Y.; Nah, Y.-C. Plasmon Enhanced Performance of Organic Solar Cells using Electrodeposited Ag Nanoparticles. *Appl. Phys. Lett.* **2008**, *93*, 073307.
(39) Garnett, E. C.; Cai, W.; Cha, J. J.; Mahmood, F.; Connor, S. T.; Christoforo, M. G.; Cui, Y.; McGehee, M. D.; Brongersma, M. L. Self-Limited Plasmonic Welding of Silver Nanowire Junctions. *Nat. Mater.* **2012**, *11*, 241−249.
(40) Cho, J. H.; Lee, J.; Xia, Y.; Kim, B.; He, Y.; Renn, M. J.; Lodge, T. P.; Frisbie, C. D. Printable Ion-Gel Gate Dielectrics for Low-Voltage Polymer Thin-Film Transistors on Plastic. *Nat. Mater.* **2008**, *7*, 900−906.
(41) Kim, S. H.; Hong, K.; Lee, K. H.; Frisbie, C. D. Performance and Stability of Aerosol-Jet-Printed Electrolyte-Gated Transistors Based on Poly(3-hexylthiophene). *ACS Appl. Mater. Interfaces* **2013**, *5*, 6580−6585.